Structure and Performance Analysis of the 7! Robots Generated From an Optimally Fault Tolerant Jacobian

Biyun Xie and Anthony A. Maciejewski, *Fellow, IEEE*

***Abstract*—A measure of local fault tolerance for kinematically redundant robots has previously been defined based on the properties of the singular values of the Jacobian matrix. Based on these measures, one can determine a Jacobian that is optimal. Because these measures are solely based on the singular values of the Jacobian, permutation of the columns does not affect the optimality. Therefore, when one generates a kinematic robot design from this optimal Jacobian, there will be 7! robot designs with the same locally optimal fault tolerant property. The work described here shows how to analyze and organize the kinematic structure of these 7! designs in terms of their Denavit and Hartenberg (DH) parameters. Furthermore, global fault tolerant measures are defined in order to evaluate the different designs. It is shown that robot designs that are very similar in terms of DH parameters, e.g., robots generated from Jacobians where the columns are in reverse order, can have very different global properties. Finally, a computationally efficient approach to calculate the global pre- and post-failure dexterity measures is presented and used to identify two Pareto optimal robot designs. The workspaces for these optimal designs are also shown.**

***Index Terms*—Failure detection and recovery, kinematics, redundant robots.**

I. Introduction

FAULT tolerant robots are defined as those robots that can still fulfill their remaining assigned tasks after a failure has occurred, without any hardware repair. These types of robots are especially useful in two situations. One is where it is difficult or dangerous to send people to repair the robot, such as space exploration [1], underwater exploration [2], and nuclear waste remediation [3], and the other is when there is no time to repair the robot, such as during surgery [4] and disaster rescue [5]. Because it is impossible to anticipate all possible failures, it is typical to design robots to be fault tolerant to the classes of failures that are most likely. The most frequently occurring failures can be categorized as locked-joint failures [6], because many failures do result in a locked joint, but also because other joint failure modes, such as free-swinging joint failures, can be transformed into this failure mode using fail-safe brakes [7].

Manuscript received February 15, 2017; accepted June 4, 2017. Date of publication June 15, 2017; date of current version June 28, 2017. This letter was recommended for publication by Associate Editor R. Ozawa and Editor P. Rocco upon evaluation of the reviewers' comments. This work was supported by the National Science Foundation under Contract IIS-0812437. *(Corresponding author: Biyun Xie.)*

The authors are with the Department of Electrical and Computer Engineering, Colorado State University, Fort Collins, CO 80523 USA (e-mail: biyunxie@rams.colostate.edu; aam@colostate.edu).

Digital Object Identifier 10.1109/LRA.2017.2715879

Kinematically redundant robots are one way to realize fault tolerance because they have more than the minimum number of degrees of freedom (DOF) to achieve their assigned tasks. Many of the previous studies on using kinematically redundant robots to achieve fault tolerance can be roughly divided into two categories, namely, design and motion planning. For example, in the design category, researchers have explored the number of DOFs that are necessary and sufficient to guarantee fault tolerance, along with how these joints should be distributed [8]. Other work has assumed a certain amount of redundancy, frequently a single additional DOF, and then developed an optimal kinematic design [9], [10] or identified an entire class of designs with the desired optimal fault tolerance property [11]–[14]. In the motion planning category, researchers frequently assume that some type of fault detection [15] and identification [16] scheme is available. Some motion planning work has focused on optimizing robot configurations in anticipation of failures [17], while others on the self-repair after a failure occurs [18]. It has also been shown that it is possible to guarantee a fault tolerant workspace by applying appropriate constraints on the motion planning algorithm [19].

The work presented here falls into the category of optimal fault tolerant kinematic design of robots with a single degree of redundancy that are used for fully general spatial positioning and orienting, i.e., 7 DOF manipulators. This letter builds on the study of [11] and [12] that will be briefly reviewed in the next section. In [11], an optimally fault tolerant Jacobian that is isotropic before failure and possesses the maximal worst-case failure tolerance after failure is developed. From the optimally fault tolerant Jacobian, a family of 7! different manipulator kinematics that locally possesses the properties of this Jacobian was generated in [12]. Then the volume of the six-dimensional workspace where the robot has a guaranteed level of fault tolerance was calculated for a few examples. However, there was not an exhaustive analysis of the global properties of the large number of robots with the desired locally optimal design. Nor has there been any taxonomy developed for the classification of robots into similar characteristics that helps to explain their global pre- and post-failure dexterity performance.

These topics are the focus of this letter. Specifically, the main contributions of this letter are as follows: (1) the characteristics of the kinematic properties, described by Denavit and Hartenberg (DH) parameters, of the 7! robots are analyzed, and used to illustrate the structural correlations between these 7! robots; (2) the global pre- and post-failure dexterity performance of the 7! robots are studied and the optimal robot designs are obtained.

2377-3766 © 2017 IEEE. Personal use is permitted, but republication/redistribution requires IEEE permission.
See http://www.ieee.org/publications_standards/publications/rights/index.html for more information.

The rest of this letter is organized as follows. In the next section the construction of the optimally fault tolerant Jacobians and the generation of the 7! fault tolerant robots from these Jacobians are reviewed. In Section III the characteristics of the DH parameters of the 7! fault tolerant robots are analyzed. In Section IV, the global pre- and post-failure dexterity performance in the joint space and in the workspace are studied, and the optimal robot designs are obtained. The conclusions of this work are presented in Section V.

II. Background on Optimally Fault Tolerant Kinematic Design

A. Definition of Optimally Fault Tolerant Jacobians[1]

The Jacobian matrix $\mathbf{J}$ of a robot is a mapping from the joint angle velocities to the end-effector velocities, which is frequently used to quantify the dexterity of a robot. For an n DOF robot working in an m dimensional workspace, the Jacobian $\mathbf{J}$ is an $m \times n$ matrix, written as a collection of columns

$$\mathbf{J}_{m\times n} = \begin{bmatrix} j_1 & j_2 & \cdots & j_n \end{bmatrix} \tag{1}$$

where j_i is the contribution of joint i to the end-effector velocity. When an arbitrary single joint f fails and is locked, the reduced Jacobian ${}^f\mathbf{J}$ can be simply obtained by removing the fth column from the original Jacobian to obtain

$${}^f\mathbf{J}_{m\times(n-1)} = \begin{bmatrix} j_1 & j_2 & \cdots & j_{f-1} & j_{f+1} & \cdots & j_n \end{bmatrix}. \tag{2}$$

In this work, failure tolerance is defined as the worst-case dexterity after an arbitrary single joint is locked. Based on this definition, a measure of the worst-case failure tolerance is given by

$$\sigma_m^* = \min_{f=1}^{n} {}^f\sigma_m \tag{3}$$

where the superscript * indicates a post-failure measure, and ${}^f\sigma_m$ is the minimal singular value of ${}^f\mathbf{J}$.

In [11], an optimally fault tolerant Jacobian is defined as follows: (1) in order to ensure that the robot has optimal dexterity performance before failure, the optimally fault tolerant Jacobian is required to be isotropic, i.e.,

$$\sigma_1 = \sigma_2 = \cdots = \sigma_m = \sigma \tag{4}$$

where the σ_i's are the singular values of the original Jacobian; (2) in order to ensure that the robot has optimal fault tolerance after failure, the optimally fault tolerant Jacobian should have the maximum value of the worst-case failure tolerance measure. Under the condition (4), the worst-case failure tolerance measure reaches its maximum value when

$${}^1\sigma_m = {}^2\sigma_m = \cdots = {}^n\sigma_m = \sigma\sqrt{\frac{n-m}{n}} \tag{5}$$

where σ is the singular value of the original Jacobian. This optimally fault tolerant Jacobian requires that each joint contributes equally to the null space, which physically means that the redundancy of the robot is uniformly distributed among all the joints so that a failure at any one joint can be compensated for by the remaining joints.

Using the above definition, the structure of an optimally fault tolerant Jacobian can be identified. For the case of a seven DOF fully spatial manipulator, the canonical optimal Jacobian is a triangular matrix where the ith row is given by:

$$\begin{aligned} j_{ik} &= 0 && \text{where} \quad k < i \\ j_{ik} &= -\sqrt{\frac{7-i}{8-i}} && \text{where} \quad k = i \\ j_{ik} &= \sqrt{\frac{1}{(7-i)(8-i)}} && \text{where} \quad k > i. \end{aligned} \tag{6}$$

Unfortunately, this canonical Jacobian cannot be realized by any manipulator built with only rotational joints. In [11], a physically realizable Jacobian for a rotary joint manipulator that is closest to optimally fault tolerant, was calculated using a numerical approach resulting in:

$$\mathbf{J}^* = \begin{bmatrix} 1 & 0.43 & 0.75 & -0.54 & 0.14 & 0.33 & -0.38 \\ 0 & -0.60 & 0.65 & 0.46 & -0.79 & -0.19 & -0.80 \\ 0 & -0.67 & -0.14 & -0.70 & 0.60 & -0.93 & -0.46 \\ 0 & 0.77 & 0.14 & 0.84 & 0.58 & -0.69 & -0.43 \\ 1 & -0.15 & -0.36 & 0.33 & -0.42 & -0.72 & 0.59 \\ 0 & 0.62 & -0.92 & -0.43 & -0.69 & -0.10 & -0.68 \end{bmatrix}. \tag{7}$$

The end-effector position and orientation at this optimally fault tolerant configuration will be referred to as the design location. The next section will show how one can identify all the physically realizable robots that possess this optimal Jacobian.

B. Generation of Robot Kinematics From Jacobians[2]

Once a Jacobian is identified, the DH parameters of a robot that possesses this Jacobian can be generated by applying the technique developed in [13]. Let v_i and ω_i denote the end-effector linear velocity and orientational velocity, respectively, due to the ith joint velocity. Each column of the Jacobian consists of these two parts, which are calculated as follows,

$$j_i = \begin{bmatrix} v_i \\ \omega_i \end{bmatrix} = \begin{bmatrix} \hat{z}_{i-1} \times p_{i-1} \\ \hat{z}_{i-1} \end{bmatrix} \forall\, i = 1, ..., n \tag{8}$$

where $\hat{z}_{i-1}$ is the unit vector along the ith joint axis, and p_{i-1} is the position vector from the $i-1$ coordinate frame to the hand coordinate frame. Consequently, all joint axes can be obtained from the rotational velocities of the Jacobian. By definition, the x axis of coordinate i is the common normal of z_{i-1} and z_i, so all x axes can be obtained after the joint axes are determined. Because all z and x axes are calculated from the Jacobian, the four DH parameters can be obtained according to their definitions.

Permuting the columns of the Jacobian changes the physical parameters of the corresponding robot but does not affect its fault

[1]The definition of optimally fault tolerant Jacobians was originally presented in [11]

[2]The generation of a family of different kinematic designs from a Jacobian was presented in [12], [13]

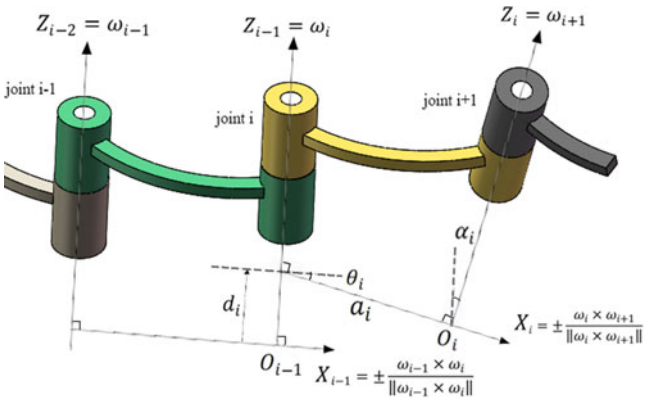

Fig. 1. The four DH parameters for each joint that specify a robot's kinematics can be obtained from the columns of a desired Jacobian, in our case the optimally fault tolerant Jacobian given in (7).

tolerance properties. Therefore, in [12] a family of 7! different robot designs was generated from the Jacobian in (7), and the 6-dimensional fault tolerant workspace volume was defined. However, only three robot designs were evaluated due to the computational complexity of the workspace calculations. The following section performs an analysis on the structure of all these 7! robots. This is followed by an analysis of their global pre- and post-failure capabilities that ultimately can be used to determine the best robot designs.

III. Characteristics of the Kinematic Parameters of the 7! Optimal Robots

A. All the Possible Values of the Four DH Parameters

By definition, DH parameter α_i is the twist angle from the z_{i-1} axis to the z_i axis about the x_i axis, and a_i is the link length, i.e., minimum distance from the z_{i-1} axis to the z_i axis along the x_i axis, as shown in Fig. 1. From the definition it can be seen that the value of α_i and a_i are both determined by the z_{i-1} axis and the z_i axis, which are obtained from two adjacent columns of a Jacobian, and the permutation of the z_{i-1} axis and the z_i axis does not affect the sign of α_i and a_i due to the convention that the x_i axis is chosen to point away from the z_{i-1} axis. Because the order does not matter, there are $C(7,2) = 21$ possible combinations to choose 2 columns from the 7 columns of the optimal Jacobian in (7) to generate two adjacent columns, so there are only 21 possible values of α and a in the 7! permutations. In addition, each α has a unique associated a, and vice versa.

Similarly, by definition, DH parameter d_i is the distance from the origin of the $i-1$ coordinate frame to the x_i axis along the z_{i-1} axis, and θ_i is the joint angle from the x_{i-1} axis to the x_i axis about the z_{i-1} axis, as shown in Fig. 1. From the definition it can be seen that the value of d_i and θ_i are both determined by the x_{i-1} axis and the x_i axis, which are obtained from the z_{i-2}, z_{i-1} and z_i axes. Because d and θ are computed based on three consecutive columns, permuting these columns will change their values. Thus, there are $P(7,3) = 210$ possible permutations to choose 3 columns from the 7 columns of the optimal Jacobian in (7), so there are 210 possible values of d and θ in the 7! permutations. In addition, each d has a unique associated θ, and vice versa.

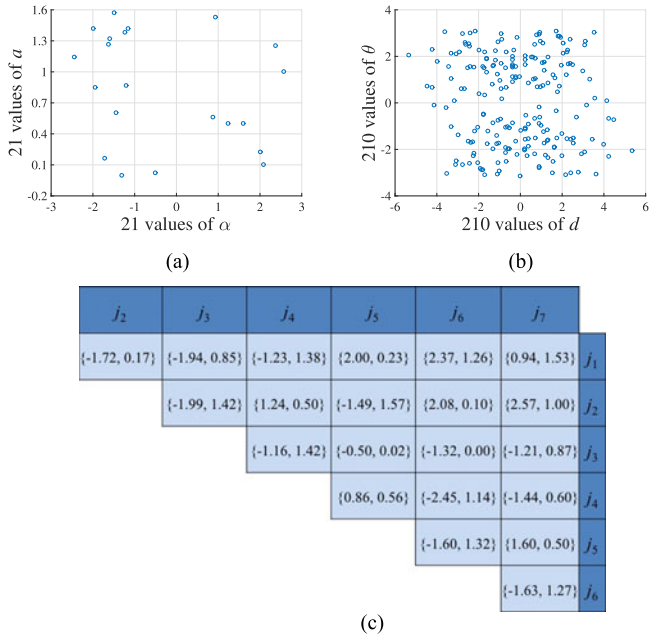

Fig. 2. In (a) are all possible 21 pairs of α and a for the 7! optimal fault tolerant robot designs. The joint pairs that generate these values are shown in (c). Note the large number of robots with α near $-\pi/2$. In (b) are all possible 210 pairs of d and θ that are symmetric with respect to the origin.

In summary, for all the DH parameters of the 7! robot designs, there are only 21 pairs of α and a, as shown in Fig. 2(a) (with the joint pairs that generate them shown in Fig. 2(c)), and they have the following properties:

1) The values of α are not uniformly distributed. In particular, there are no α's near 0, and there is a big gap between -0.50 and 0.86, because if joints i and k are parallel then $\omega_i = \omega_k$ so that j_i and j_k will have similar contributions to the end effector velocity, which is not beneficial for dexterity or fault tolerance. In contrast, there are many α's near $\pm\pi/2$, because if joint i is orthogonal to joint k then $\omega_i \perp \omega_k$ so that j_i and j_k are more likely to maintain the optimal angular separation for fault tolerance.
2) The values of a vary from 0.00 to 1.57, which makes sense because a can not be greater than 2. This is true because at the optimally fault tolerant configuration all the joints are constrained to lie on a unit sphere that is centered at the end effector, and a is the distance between two joint axes, which can not be larger than the diameter of the unit sphere.

There are 210 pairs of d and θ, as shown in Fig. 2(b), and they have the following properties:

1) For each pair of d and θ there exists a pair $-d$ and $-\theta$ that is symmetric with respect to the origin. This is because the permutations of two x axes affect the sign of d and θ, but not the value.
2) In contrast to the link length a, the values of d vary from -5.35 to 5.35, and are not limited to 2. In fact, because d is the distance between the location of the two common normals before and after its joint axis, it can theoretically

be from $-\infty$ to ∞, however, d is limited because of the properties of α.

It is important to point out that the DH parameters for a given robot's kinematic structure are not unique. For example, one can take the negative of any column of the Jacobian and the DH parameters will change, however, the robot's kinematic structure and its fault tolerant properties will not. In particular, taking the negative of the ith column of the Jacobian changes the values of α_{i-1} and α_i by adding π (if α_{i-1} or α_i is negative) or subtracting π (if α_{i-1} or α_i is positive). The signs of d_i and θ_i will also change.

B. Organization of the Seven Sets of DH Parameters for Each Robot

In Section III-A, all the possible DH parameters of the 7! robot designs generated from the optimally fault tolerant Jacobian in (7) were determined. In this section, we illustrate how the DH parameters for each of the seven joints of a robot can be obtained by selecting from the above possible values.

As stated in Section III-A, there are 21 possible values for each individual α_i and a_i. Because selecting one determines the other, we will denote the pair as $\{\alpha_i, a_i\}$ to emphasize that they can not be separated. In addition, it is important to recall that once an $\{\alpha_i, a_i\}$ is selected, this implies that two specific columns of the Jacobian, say j_a and j_b must be adjacent (see Fig. 2(c)), but the order does not matter. We will denote this with the ordered pairs (j_a, j_b) and (j_b, j_a). Also, whenever $\{\alpha_{i+1}, a_{i+1}\}$ is selected, note that its associated ordered pair must contain one Jacobian column from the order pair of the previous $\{\alpha_i, a_i\}$.

We now describe the possibilities for determining all seven sets of DH parameters of an optimal robot. The value of $\{\alpha_1, a_1\}$ can be chosen freely from the 21 possible choices. Once the value of $\{\alpha_1, a_1\}$ is determined, the first two columns of the associated Jacobian (j_a, j_b) or (j_b, j_a) are determined. Thus there are now two possibilities for j_2. These two possibilities can be paired with five remaining choices for j_3 so that there are ten possibilities for $\{\alpha_2, a_2\}$. The choices for remaining $\{\alpha_i, a_i\}$'s can be determined in an analogous manner. In particular, the number of possible choices for $\{\alpha_3, a_3\}$ ... $\{\alpha_6, a_6\}$ are 4, 3, 2, and 1, respectively. The value of $\{\alpha_7, a_7\}$ is arbitrary because the end-effector coordinate frame is arbitrary. In [13], α_7 is set to be 0, and a_7 is set to be 1. The organization of all the 7 sets of $\{\alpha_i, a_i\}$ is a tree structure, as shown in Fig. 3.

C. Correlations Between the DH Parameters of Two Reverse Version Robot Designs

For any robot design from the 7! robots whose associated Jacobian is $\mathbf{J}^{\mathrm{l}} = \begin{bmatrix} j_{\mathrm{l}_1} & j_{\mathrm{l}_2} & j_{\mathrm{l}_3} & j_{\mathrm{l}_4} & j_{\mathrm{l}_5} & j_{\mathrm{l}_6} & j_{\mathrm{l}_7} \end{bmatrix}$, there exists a reverse version of this robot whose associated Jacobian is $\mathbf{J}^{\mathrm{r}} = \begin{bmatrix} j_{\mathrm{l}_7} & j_{\mathrm{l}_6} & j_{\mathrm{l}_5} & j_{\mathrm{l}_4} & j_{\mathrm{l}_3} & j_{\mathrm{l}_2} & j_{\mathrm{l}_1} \end{bmatrix}$, where "l" indicates left to right order, and "r" is the reverse. Based on the analysis in Subsection A, these two robot designs have the same α's and a's, but they are in reverse order, i.e., $\alpha_1^{\mathrm{l}} = \alpha_6^{\mathrm{r}}$, $a_1^{\mathrm{l}} = a_6^{\mathrm{r}}$, ..., $\alpha_6^{\mathrm{l}} = \alpha_1^{\mathrm{r}}$, $a_6^{\mathrm{l}} = a_1^{\mathrm{r}}$. These two robot designs have d's and θ's that are of opposite sign, and they are also in reverse order, i.e., $d_2^{\mathrm{l}} = -d_6^{\mathrm{r}}$, $\theta_2^{\mathrm{l}} = -\theta_6^{\mathrm{r}}$, ..., $d_6^{\mathrm{l}} = -d_2^{\mathrm{r}}$, $\theta_6^{\mathrm{l}} = -\theta_2^{\mathrm{r}}$. Fig. 4 shows two reverse version robot designs. It can be seen that although these two robots have very similar DH parameters, they have different structures, and it will be shown in the next section that the global properties of these two reverse version robots is quite different, although this is not typically the case.

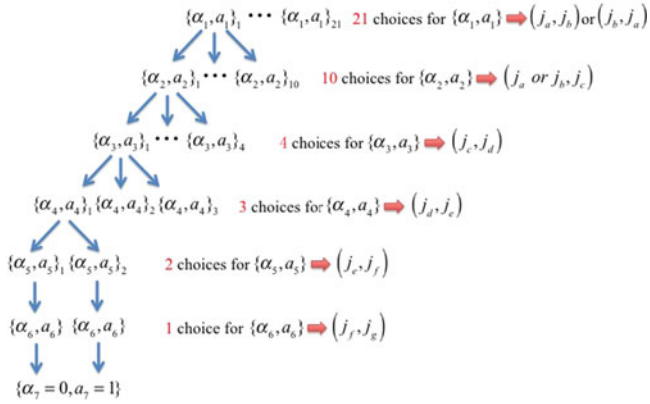

Fig. 3. The tree structure of the 7 sets $\{\alpha_i, a_i\}$ of each robot design.

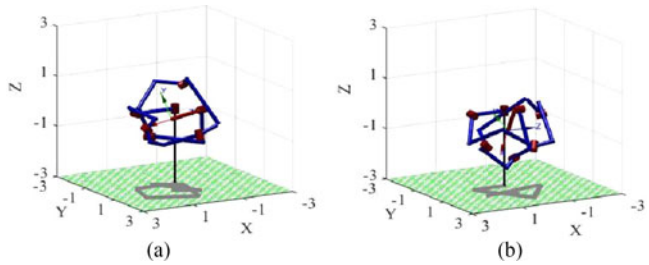

Fig. 4. Two reverse version robot designs that have very different global properties. Note how all of the joint axes are tangent to a sphere of unit radius about the end effector position, as is required for an optimally fault tolerant configuration. (This depiction of the robot kinematics is meant to illustrate these properties and not to represent how the robot would be manufactured.)

IV. Global Pre- and Post-Failure Dexterity of the 7! Robot Designs

A. Overview

All these 7! robot designs possess the locally optimal fault tolerant Jacobian at a specific optimal configuration, so they have the same optimal local performance with the end effector at the optimal design location. However, it is important to also consider the global performance of a robot design. In [12], a global measure of a robot's 6-dimensional fault tolerant workspace volume was proposed, but only the global performance of three robot designs was studied due to the computational complexity. In this section, the global pre- and post-failure dexterity performance of all 7! robot designs are studied, and based on these results, the optimal robot designs are identified.

B. Correlations Between Common Pre- and Post-Failure Dexterity Measures

The pre-failure dexterity performance is evaluated by using the following three commonly used measures, i.e., minimal

TABLE I
THE CORRELATIONS BETWEEN THE LOCAL PRE- AND POST-FAILURE DEXTERITY MEASURES

	$1/\kappa$	w	σ_m	$1/\kappa^*$	w^*	σ_m^*
$1/\kappa$	1.000	0.748	0.992	0.401	0.439	0.401
w	0.748	1.000	0.773	0.342	0.604	0.357
σ_m	0.992	0.773	1.000	0.398	0.454	0.405
$1/\kappa^*$	0.401	0.342	0.398	1.000	0.817	0.996
w^*	0.439	0.604	0.454	0.817	1.000	0.825
σ_m^*	0.401	0.357	0.405	0.996	0.825	1.000

singular value σ_m, the condition number κ, and manipulability w, which are defined as

$$\kappa = \frac{\sigma_1}{\sigma_m} \quad \text{and} \tag{9}$$

$$w = \sigma_1 \sigma_2 \cdots \sigma_m . \tag{10}$$

We will use the reciprocal of κ to make the measure be between 0 and 1. The post-failure dexterity performance is frequently measured by the worst-case value of the above three dexterity measures after an arbitrary joint is locked, i.e.,

$$\kappa^* = \min_{f=1}^{n} {}^f\kappa, \tag{11}$$

$$w^* = \min_{f=1}^{n} {}^f w, \tag{12}$$

and σ_m^* is defined as in (3), where ${}^f\kappa$ and ${}^f w$ are the condition number and manipulability, respectively, after joint f is locked. In order to eliminate the difference in units between linear velocity and rotational velocity, the first three rows of the Jacobian are normalized by the maximal distance that this robot can reach, before calculating these measures.

In order to study the correlations between these six pre- and post-failure dexterity measures, 10,000 configurations are randomly sampled in the joint space of the robot design generated from the Jacobian in (7). The correlation coefficient between each of the measures is shown in Table I. The three pre-failure dexterity measures are highly correlated with each other, especially the inverse condition number and minimal singular value, and this is also true for the three post-failure dexterity measures. However, the correlations between the pre- and post-failure dexterity measures are relatively low. In the sub correlation coefficient matrix of the three pre-failure dexterity measures, the column of σ_m has the largest norm, which means that σ_m is the most representative measure to evaluate the pre-failure dexterity performance of the robot designs. Similarly, σ_m^* is the most representative measure among the three post-failure dexterity measures. Fig. 5 shows the values of σ_m and σ_m^* at all 10,000 sampled configurations. It can be seen that the configurations with a small σ_m must also have a small σ_m^*, however, the reverse is not true. This indicates that σ_m^* is really a measure of a different property. For the remainder of this work σ_m and σ_m^* are used to evaluate the global pre- and post-failure dexterity performance of the 7! robot designs.

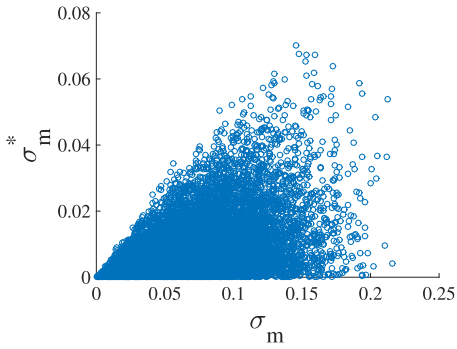

Fig. 5. The values of σ_m and σ_m^* for 10,000 samples in the joint space for the robot generated from (7). Note that σ_m^* is bounded by σ_m, and can take any value down to zero even for large σ_m.

C. Correlations Between the Global Pre- and Post-Failure Dexterity in the Joint Space and in the Workspace

There are two ways to approximate the average global performance of a robot, i.e., sampling in the joint space or sampling in the workspace. One can estimate the average global dexterity in the joint space by simply evaluating the dexterity measures at randomly generated configurations and taking the average. That is, the global σ_m and σ_m^* in the joint space are calculated using

$$\bar{\sigma}_m = \frac{\sum_{i=1}^{N} \sigma_m}{N} \quad \text{and} \tag{13}$$

$$\bar{\sigma}_m^* = \frac{\sum_{i=1}^{N} \sigma_m^*}{N} \tag{14}$$

where $\bar{\sigma}_m$ is the average dexterity, $\bar{\sigma}_m^*$ is the average fault tolerance, and N is the number of samples. Clearly the accuracy of the average global measure increases with N, however, so does the computation time. As a compromise between accuracy and computation time, $N = 10,000$ is used when sampling in the joint space. Based on our analysis this results in an error of $\approx$3% for global σ_m and $\approx$5% for global σ_m^*.

In contrast to sampling in the joint space, the calculation of the global measure in the workspace is much more difficult and time consuming, because at each location in the workspace, there are multiple configurations that have different local dexterity performance. One can assume that an inverse kinematics routine that optimizes the desired dexterity measure is being used. Therefore, it makes sense to quantify the dexterity measure at a workspace location using the maximum value over all configurations at that location. This requires the following steps: (a) A number of locations (position and orientation) are randomly sampled in the 6-dimensional workspace by the direct sampling method in [12]. (b) All the self-motion manifolds at each location are calculated, and the local σ_m and σ_m^* along these self-motion manifolds are obtained. (c) The maximal σ_m and σ_m^* are saved as the optimal pre- and post-failure dexterity performance at this location. (d) Finally, the global σ_m and σ_m^* in the workspace can be calculated using (13) and (14) based on these optimal σ_m and σ_m^* found at each sample location. For sampling in the workspace $N = 5000$ is used due to the greater computational complexity. This results in an error of $\approx$2% for

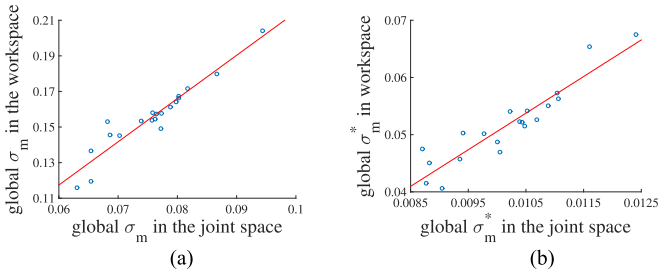

Fig. 6. The correlations between global measures in the joint space and in the workspace where (a) is the global σ_m and (b) is the global σ_m^*.

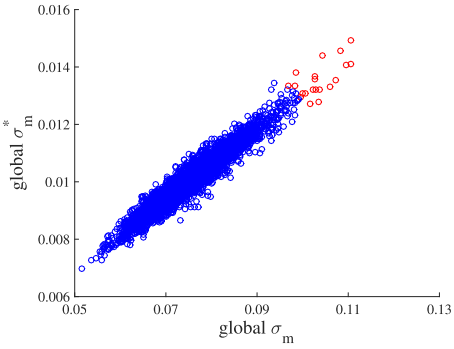

Fig. 7. The global σ_m and σ_m^* of the 7! robots in the joint space.

both global σ_m and σ_m^*. It may at first seem strange that a higher accuracy is obtained with a lower number of samples as compared to sampling in the joint space. However, this is due to the fact that an optimization is done at each workspace location to identify the optimal value, which are then averaged.

When robots are applied for a particular task, one is usually more interested in a robot's performance in the workspace. Therefore, robot designers would typically prefer a measure of the workspace dexterity. However, as discussed above, this is much more computationally expensive, especially when it needs to be evaluated for 7! robot designs. If it can be shown that there is a correlation between the measures computed in the joint space and those in the workspace, then the more computationally efficient joint-space computations can be used to identify a smaller number of optimal robot design candidates on which the more computationally expensive workspace analysis can be performed.

To see if joint space measures are correlated to workspace measures, 20 robot designs are randomly chosen from the 7! robots, and their global σ_m and σ_m^* are calculated. Fig. 6 shows the global σ_m and σ_m^* both in the joint space and in the workspace. There is a relatively strong linear correlation between the joint space measures and the workspace measures. The linear correlation coefficient between the global σ_m in the joint space and in the workspace is 0.74, and the linear correlation coefficient between the global σ_m^* in the joint space and in the workspace is 0.71. This means that one can use the joint-space measures as an approximation for the workspace measures to select optimal robot design candidates.

D. Global Pre- and Post-Failure Dexterity of the 7! Optimal Robots in the Joint Space

Based on the relatively strong linear correlation obtained in the above section, the robot designs with optimal global dexterity performance in the joint space are more likely to have optimal global dexterity performance in the workspace. Therefore, the global pre- and post-failure dexterity performance of all the 7! robots are first calculated in the joint space to find the robot designs with optimal global joint space measures. These robots will be the optimal robot design candidates.

Fig. 7 shows the global σ_m and σ_m^* of all the 7! robot designs in the joint space. As discussed in Section III, there are some relationships between specific DH parameters and good local

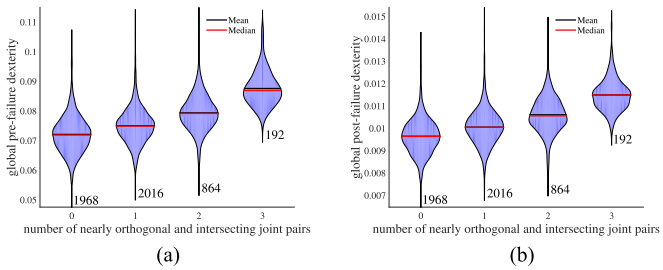

Fig. 8. Robots that contain a larger number of nearly orthogonal and intersecting joint pairs are more likely to have high global pre- and post-failure dexterity. The 7! robots have been grouped based on the number of such joint pairs, and the distribution of their global pre- and post-failure dexterities are shown in (a) and (b), respectively. The number next to the distribution indicates the numbers of robots in each group.

pre- and post-failure dexterity measures. Reformatting the data in Fig. 7 reveals additional correlations with global properties, i.e., that nearly orthogonal joints with small link lengths are more likely to generate robots with good global pre- and post-failure dexterity. There are three joint pairs, out of the 21 possible pairs, that nearly satisfy these conditions, i.e., the $\{\alpha, a\}$ pairs $\{-1.32, 0.00\}$, $\{-1.72, 0.17\}$ and $\{1.60, 0.50\}$. One can classify each of the 7! robot designs into four groups according to how many of these $\{\alpha, a\}$ pairs they contain. The distribution of global pre- and post-failure dexterity performance in the joint space of these groups is shown in Fig. 8. It is easy to see that the mean dexterity performance increases as the number of good pairs increases, and even the worst robot in the group with three pairs has relatively good global pre- and post-failure dexterity. However, one must be careful because the order of the DH parameters also matters. Every one of the 7! robot designs has a reverse version that has very similar DH parameters, but in reverse order. The global performance of the two can be quite different, as shown in Fig. 9 where this difference is plotted for all 7!/2 pairs.

The red points in Fig. 7 are the 20 optimal robot design candidates, which have optimal global pre- and post-failure dexterity performance in the joint space. None of the remaining robot designs have both better global pre- and post-failure dexterity than these 20 candidates. Based on the analysis in the above section, it is likely that these 20 candidates have better global performance in the workspace than the remaining robot designs, so

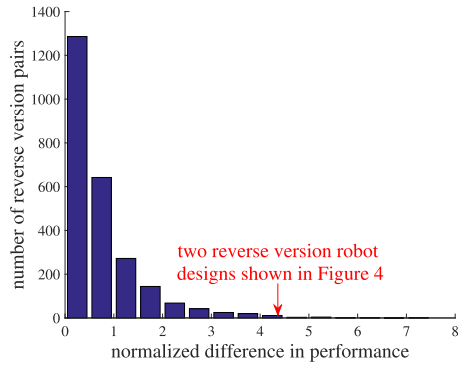

Fig. 9. The distribution of the difference in performance between a robot design and its reverse version is shown. The difference is computed as the Euclidean distance between the normalized pre- and post-failure measures.

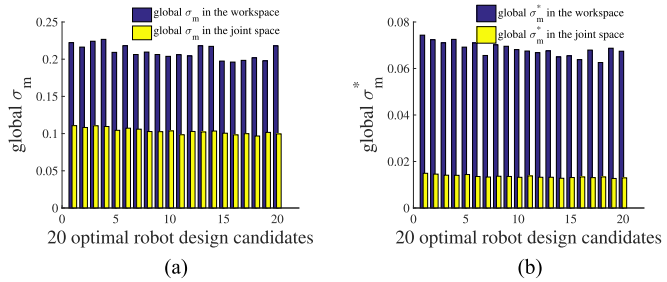

Fig. 10. The global measures of the 20 optimal robot design candidates in the joint space and in the workspace where (a) is the global σ_m and (b) is the global σ_m^*.

only the global performance of these 20 robot designs are calculated in the workspace. These top 20 robot designs are ordered (somewhat arbitrarily) by the sum of their normalized global σ_m and σ_m^*.

E. Global Pre- and Post-Failure Dexterity of the 20 Candidates in the Workspace

The global dexterity performance of the 20 optimal robot design candidates are calculated in the workspace. Both the global joint space measures and the global workspace measures of the 20 candidates are shown in Fig. 10. Clearly, the global measures in the workspace are much better than those in the joint space, because at each location the configurations with the optimal measures at this location are identified. Fig. 11 shows the Pareto frontier when the two objective functions are global σ_m and σ_m^*. Among the 20 robot design candidates, Candidate 4, that results from the permutation $\left[\, j_7 \;\; j_4 \;\; j_5 \;\; j_1 \;\; j_2 \;\; j_6 \;\; j_3 \,\right]$, has the best global pre-failure dexterity in the workspace, and Candidate 1, that results from the permutation $\left[\, j_6 \;\; j_7 \;\; j_3 \;\; j_5 \;\; j_2 \;\; j_1 \;\; j_4 \,\right]$, has the best global post-failure dexterity in the workspace, where j_i is the ith column of the optimal Jacobian in (7). These two optimal robot designs are shown in their optimally fault tolerant configurations in Fig. 12.

The pre- and post-failure dexterity measures throughout the workspace for the two optimal robot designs are shown in Fig. 13. Because of the difficulty of representing and visualizing a 6-dimensional workspace, only the performance in their

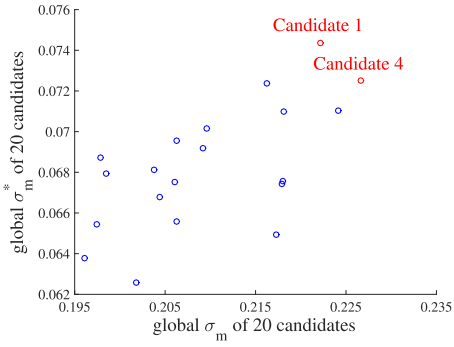

Fig. 11. The global values of σ_m and σ_m^* computed in the workspace are shown for the 20 optimal robot design candidates. Candidates 1 and 4 represent the Pareto solutions to this bi-objective optimization.

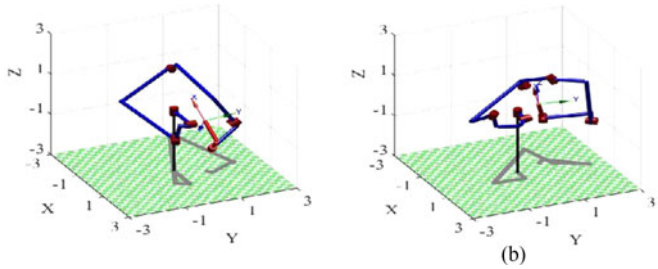

Fig. 12. The optimal robot designs in their optimal configuration where (a) is the Candidate 1 robot design and (b) is the Candidate 4 robot design.

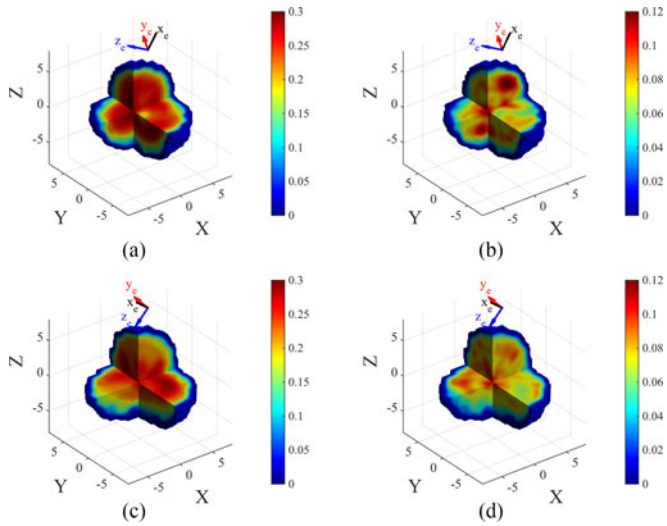

Fig. 13. The pre- and post-failure dexterity performance in the 3-dimensional position workspace are shown for Candidate robot designs 1 and 4, where both are constrained to be at the orientation of the optimal design point. Pre- and post-failure dexterity performance of Candidate 4 are shown in (a) and (b), respectively, and Candidate 1 in (c) and (d), respectively.

3-dimensional position workspace is plotted by constraining the orientation to be that of the optimal design configuration. In order to show the dexterity performance in the interior of the workspace, the 3-dimensional position workspace is shown with multiple cross-sections at the design point. Fig. 13(a) and (b) are the pre- and post-failure dexterity performance, respectively, of the Candidate 4 robot design, and Fig. 13(c) and (d) are

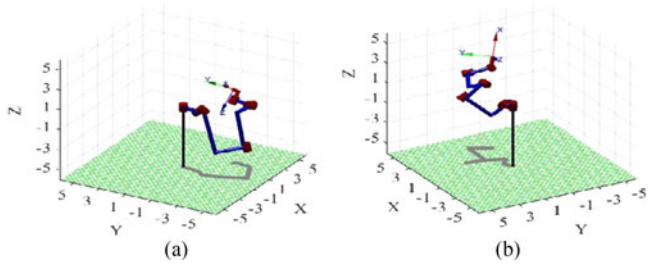

Fig. 14. The configurations of the optimal robot designs at the locations where the fault tolerance measure is 90% of the maximum value are shown in (a) for Candidate 1 and (b) for Candidate 4.

the pre- and post-failure dexterity performance, respectively, of Candidate 1. From the figure, one can see that neither σ_m nor σ_m^* reaches its maximum value at the center point. This is because at this design location the robots are required to be both isotropic and fault tolerant. At other points, the robots are no longer constrained to be isotropic so that the values of σ_m and σ_m^* can be higher. Note that the volume of high pre-failure dexterity is much more uniform than that of post-failure dexterity. To illustrate the high levels of pre- and post-failure dexterity that can be maintained over a large portion of the workspace, Fig. 14 shows the configurations of Candidate 1 and 4 robot designs at the location where the fault tolerance measure is 90% of the maximum value.

V. Conclusion

This work explored the structure and global pre- and post-failure dexterity performance of the 7! robot designs generated from an optimally fault tolerant Jacobian. It was shown that when describing the kinematic design of a robot in terms of DH parameters for all joints, there are only 21 possible values of α and a for all 7! robot designs, and there are 210 possible values of d and θ. In addition, these designs were organized into a tree structure based on the possible choices for $\{\alpha, a\}$ pairs. It was also shown that each of the 7! robot designs had a reverse version with very similar DH parameters but potentially very different global properties. Furthermore, the global performance of the 7! robot designs was analyzed. It was shown that there is a relatively strong correlation between performance measures computed in the joint space and workspace, so that the computationally efficient joint space calculations could be used to identify the best candidates for optimal designs in the workspace. These candidates were further analyzed in the workspace to determine two Pareto optimal designs in terms of pre- and post-failure dexterity, and the distribution of these measures throughout the workspace were shown.

References

[1] Z. Mu, B. Zhang, W. Xu, B. Li, and B. Liang, "Fault tolerance kinematics and trajectory planning of a 6-DOF space manipulator under a single joint failure," in *Proc. IEEE Int. Conf. Real-Time Comput. Robot.*, 2016, pp. 483–488.

[2] S. Soylu, B. J. Buckham, and R. P. Podhorodeski, "Redundancy resolution for underwater mobile manipulators," *Ocean Eng.*, vol. 37, no. 2–3, pp. 325–343, 2010.

[3] J. Trevelyan, W. R. Hamel, and S.-C. Kang, "Robotics in hazardous applications," in *Springer Handbook of Robotics*. New York, NY, USA: Springer, 2016, pp. 1521–1548.

[4] M. Y. Jung, R. H. Taylor, and P. Kazanzides, "Safety design view: A conceptual framework for systematic understanding of safety features of medical robot systems," in *Proc. IEEE Int. Conf. Robot. Autom.*, 2014, pp. 1883–1888.

[5] K. Nagatani *et al.*, "Emergency response to the nuclear accident at the Fukushima Daiichi Nuclear Power Plants using mobile rescue robots," *J. Field Robot.*, vol. 30, no. 1, pp. 44–63, 2013.

[6] H. Chang, P. Huang, M. Wang, and Z. Lu, "Locked-joint failure identification for free-floating space robots," in *Proc. IEEE Int. Conf. Inf. Autom.*, 2014, pp. 170–175.

[7] J. D. English and A. A. Maciejewski, "Fault tolerance for kinematically redundant manipulators: Anticipating free-swinging joint failures," *IEEE Trans. Robot. Autom.*, vol. 14, no. 4, pp. 566–575, Aug. 1998.

[8] C. J. Paredis and P. K. Khosla, "Designing fault-tolerant manipulators: How many degrees of freedom?" *Int. J. Robot. Res.*, vol. 15, no. 6, pp. 611–628, 1996.

[9] Q. Li and J. Zhao, "A universal approach for configuration synthesis of reconfigurable robots based on fault tolerant indices," *Ind. Robot, Int. J.*, vol. 39, no. 1, pp. 69–78, 2012.

[10] C. S. Ukidve, J. E. McInroy, and F. Jafari, "Using redundancy to optimize manipulability of stewart platforms," *IEEE/ASME Trans. Mechatronics*, vol. 13, no. 4, pp. 475–479, Aug. 2008.

[11] A. A. Maciejewski and R. G. Roberts, "On the existence of an optimally failure tolerant 7R manipulator Jacobian," *Appl. Math. Comput. Sci.*, vol. 5, no. 2, pp. 343–357, 1995.

[12] K. M. Ben-Gharbia, A. A. Maciejewski, and R. G. Roberts, "Kinematic design of manipulators with seven revolute joints optimized for fault tolerance," *IEEE Trans. Syst., Man, Cybern., Syst.*, vol. 46, no. 10, pp. 1364–1373, Oct. 2016.

[13] K. M. Ben-Gharbia, A. A. Maciejewski, and R. Roberts, "An illustration of generating robots from optimal fault-tolerant Jacobians," in *Proc. 15th IASTED Int. Conf. Robot. Appl.*, 2010, pp. 1–3.

[14] Y. Yi, J. E. McInroy, and F. Jafari, "Generating classes of locally orthogonal Gough-Stewart platforms," *IEEE Trans. Robot.*, vol. 21, no. 5, pp. 812–820, Oct. 2005.

[15] W. E. Dixon, I. D. Walker, D. M. Dawson, and J. P. Hartranft, "Fault detection for robot manipulators with parametric uncertainty: A prediction-error-based approach," *IEEE Trans. Robot. Autom.*, vol. 16, no. 6, pp. 689–699, Dec. 2000.

[16] M. L. McIntyre, W. E. Dixon, D. M. Dawson, and I. D. Walker, "Fault identification for robot manipulators," *IEEE Trans. Robot.*, vol. 21, no. 5, pp. 1028–1034, Oct. 2005.

[17] K. N. Groom, A. A. Maciejewski, and V. Balakrishnan, "Real-time failure-tolerant control of kinematically redundant manipulators," *IEEE Trans. Robot. Autom.*, vol. 15, no. 6, pp. 1109–1115, Dec. 1999.

[18] A. Cully, J. Clune, D. Tarapore, and J.-B. Mouret, "Robots that can adapt like animals," *Nature*, vol. 521, no. 7553, pp. 503–507, 2015.

[19] R. C. Hoover, R. G. Roberts, A. A. Maciejewski, P. S. Naik, and K. M. Ben-Gharbia, "Designing a failure-tolerant workspace for kinematically redundant robots," *IEEE Trans. Autom. Sci. Eng.*, vol. 12, no. 4, pp. 1421–1432, Oct. 2015.